
Effects of materials parameters on mineralization and degradation of sol-gel bioactive glasses with 3D-ordered macroporous structures

Kai Zhang,¹ Hongwei Yan,² David C. Bell,^{3*} Andreas Stein,² Lorraine F. Francis¹

¹Department of Chemical Engineering and Materials Science, University of Minnesota, Minneapolis, Minnesota 55455

²Department of Chemistry, University of Minnesota, Minneapolis, Minnesota 55455

³Institute of Technology Characterization Facility, University of Minnesota, Minneapolis, Minnesota 55455

Received 6 August 2002; revised 19 November 2002; accepted 24 February 2003

Abstract: Bioactive glasses (BGs) with three-dimensionally ordered macroporous (3DOM) structures were prepared by combining a sol-gel synthesis with colloidal crystal templating. 3DOM sol-gel BGs with two compositions (20 mol % CaO–80% SiO₂ and 20 mol % CaO–4% P₂O₅–76% SiO₂) and three macropore sizes (average: 345, 440, and 790 nm) were prepared. Glasses were separated into two particle sizes (212 μm < small < 355 μm and 600 μm < large < 1000 μm). The glasses were soaked in simulated body fluid at 37°C for 2 or 4 days and the effects of composition, particle size, and macropore size on the formation of apatite and glass degradation were characterized. Within the parameter range of the experiments, several comparisons could be made. First,

the formation of apatite and degradation of the glass were slightly enhanced for the phosphate containing composition. Second, large particles formed less apatite and degraded less completely compared with small particles. Lastly, an increase in macropore size slowed down the glass degradation and apatite formation processes, an effect related to the decreased internal surface area of the larger pore materials. © 2003 Wiley Periodicals, Inc. *J Biomed Mater Res* 66A: 860–869, 2003

Key words: macroporous; sol-gel; bioactive glass; apatite; mineralization; simulated body fluid (SBF); pore size; particle size

INTRODUCTION

Bioactive glasses (BGs) and glass-ceramics form a chemical bond to bone through a biologically active apatite layer that forms on their surfaces.¹ Consequently, these materials have found a variety of applications, including mid-ear and bone implants, artificial vertebrae, orthopedic coating materials, and components in bioactive composites.^{1–5} Bioactive ma-

terials that are also biodegradable have recently gained attention as candidate materials for *in vivo* tissue regeneration and tissue engineering scaffolds.⁶ Hench and Polak⁷ termed these bioactive and biodegradable materials as third generation biomaterials, following the first generation of bioinert materials, and the second generation of more interactive materials such as bioactive ceramics and biodegradable polymers. In the quest for this new generation of materials, bioactive glasses with tailored compositions and structures, at various length scales, hold promise. Sol-gel processing is an ideal route to achieve compositional and structural control.

Sol-gel processing, an alternative to traditional melt processing of glasses, involves the synthesis of a solution (sol), typically composed of metalorganic and metal salt precursors, followed by the formation of a gel by chemical reaction or aggregation, and lastly thermal treatment for drying, organic removal, and sometimes crystallization.⁸ Compared with conventional melt-processed BGs, sol-gel BGs are processed at lower temperatures and have better compositional control.^{3,9,10} Additionally, sol-gel BGs are more easily created with the combination of bioactivity and bio-

*Present address: Center for Imaging and Mesoscale Structures, Harvard University, 7 Divinity Avenue, Cambridge, MA 02138.

Correspondence to: L. F. Francis; e-mail: lfrancis@tc.umn.edu
Contract grant sponsor: MRSEC program of the National Science Foundation; contract grant numbers: DMR-9809364 and DMR-9701507

Contract grant sponsor: David & Lucile Packard Foundation

Contract grant sponsor: U.S. Army Research Laboratory
Contract grant sponsor: U.S. Army Research Office; contract grant number: DAAD 19-01-1-0512

Contract grant sponsor: Office of Naval Research; contract grant number: N00014-01-1-0810, subcontracted from NWU.

degradability. Results from both *in vitro* studies in acellular simulated body fluid (SBF)^{9–12} and *in vivo* tests in animal models^{13–15} demonstrate that sol-gel derived BGs are more bioactive (as represented by the induction time of apatite) and degradable (as represented by the amount of residual glass) than BGs made by conventional melt processes. Sol-gel BGs also have other potential applications, such as delivery of drugs or biological molecules^{16–18} and as particulate fillers for *in situ* tissue regeneration.^{6,7}

A key feature of bioactive materials is their ability to form bone-like apatite on their surfaces *in vivo* and *in vitro*. The *in vitro* studies of apatite formation are carried out by soaking the glass at body temperature in an aqueous solution with pH and ionic composition similar to that of blood plasma.¹⁹ The sequence of events leading to apatite formation includes release of ions from the glass, formation and condensation of silanol groups on the glass surface, adsorption of calcium and phosphate ions to the surface to nucleate an amorphous calcium phosphate, and growth and crystallization of the calcium phosphate layer.¹ For sol-gel BGs, the synthetic route and lower heating temperatures lead to increased numbers of silanol groups^{9,10,20} and/or mesopores,^{21,22} both of which may act as nucleation sites for apatite formation.

In vitro apatite formation is affected by a number of variables, including ion concentration, pH,²³ circulation of the *in vitro* soaking solution,²⁴ the choice of precursor,^{11,25} glass composition,^{26–29} processing temperature,^{9,30–32} and texture (pore size and volume).^{21,22,33–39} Glass compositions affect apatite formation through chemical influences (retardation from MgO²⁷ and enhancement from P₂O₅²⁶) and/or structural changes (porosity and surface area variations due to relative contents of SiO₂ and CaO³⁷). The glass preparation temperature affects the glass structure, texture, and chemistry, which in turn affect the activation energy for ion release and the apatite formation process.^{9,30–32} It has also been shown that microporous and mesoporous (<50 nm) textures of the sol-gel BGs encourage apatite mineralization and glass degradation.^{12,21,22,34,37,38} However, few investigations have focused on the preparation or properties of sol-gel BGs with voids on the macropore (>50 nm) length scale.^{6,30}

We previously reported a new method for the preparation of a sol-gel-derived BG with ordered, interconnected macropores (average pore diameter: 410 nm) and a uniform pore size distribution.³⁰ The synthesis of these so-called three-dimensionally ordered macroporous (3DOM) sol-gel BGs is adapted from the colloidal crystal templating method used to create novel photonic materials.⁴⁰ 3DOM sol-gel BGs with a composition of 20 mol % CaO–80% SiO₂ have been demonstrated to form apatite and degrade faster in SBF at body temperature than conventional sol-gel BGs. This

behavior was attributed to the unique structure and higher accessible surface area for 3DOM sol-gel BGs. For samples calcined at 600°C, bone-like apatite was fully developed throughout the porous structure within 4 days of soaking in SBF, concomitant with the degradation of the 3DOM structure.³⁰ Interestingly, because the glasses were calcined at higher temperatures (up to 800°C), a longer soaking time in SBF was needed to initiate the formation of an apatite layer. Because the surface area and porosity did not change significantly with calcination temperature, the decreased activity of these glasses appears to be linked to the decreasing silanol content in the glass. In addition to calcination temperature, many other parameters can affect the degradation and apatite formation of 3DOM sol-gel BGs, and an understanding of these parameters is necessary to optimize 3DOM sol-gel BGs for potential applications in tissue regeneration and delivery of biological factors. In these applications, bone tissue ingrowth is not required and the pore size does not need to meet the typical ~100- μ m limit. Instead, the interconnected, macroporous structure and controlled degradability of 3DOM sol-gel BG particulates is desirable.

In this report, we continue the study of the mineralization and degradation of 3DOM sol-gel BGs with an emphasis on the effects of material parameters. For this purpose, 3DOM sol-gel BGs with different particle sizes, macropore sizes, and chemical compositions were prepared. A series of comparative studies were conducted using Fourier-transform infrared (FTIR) spectroscopy, powder X-ray diffraction (XRD), scanning electron microscopy (SEM), transmission electron microscopy (TEM), N₂ adsorption, and inductive coupled plasma (ICP) atomic emission spectroscopy as characterization techniques.

MATERIALS AND METHODS

Materials

Tetraethylorthosilicate (TEOS), Ca(NO₃)₂ · 4H₂O, triethyl phosphate (TEP), reagent-grade chemicals NaCl, NaHCO₃, KCl, K₂HPO₄ · 3H₂O, MgCl₂ · 6H₂O, CaCl₂, tris(hydroxymethyl) aminomethane [Tris-buffer, (CH₂OH)₃CNH₂], and 1M HCl were purchased from Aldrich Inc. Monodisperse poly(methyl methacrylate) (PMMA) latex spheres with different sizes were synthesized and packed into colloid crystals of centimeter-scale by centrifugation, as described before.^{41,42}

Preparation of 3DOM sol-gel bioactive glasses

CaO–SiO₂ 3DOM sol-gel BGs were prepared according to the procedure described previously.³⁰ Briefly, Ca(NO₃)₂ ·

TABLE I
Material Parameters of 3DOM Sol-gel BGs

Sample	Composition (mol %)	Macropore Size (nm) ^a	Glass Particle Size ^b
345-s-P	20 CaO–4 P ₂ O ₅ –76 SiO ₂	345	Small
345-s	20 CaO–80 SiO ₂	345	Small
345-l	20 CaO–80 SiO ₂	345	Large
440-s	20 CaO–80 SiO ₂	440	Small
790-s	20 CaO–80 SiO ₂	790	Small

^aAverage values based on SEM observations

^b212 μm < small < 355 μm; 600 μm < large < 1000 μm.

4H₂O was dissolved in 1M HNO₃ solution and TEOS was added to the solution with vigorous stirring to obtain a nominal composition of 20 mol % CaO–80% SiO₂. After 10–15 min of hydrolysis under stirring, a homogenous sol was obtained. Stirring was stopped and centimeter-scale, close-packed PMMA colloidal crystals were added to the solution. After 3–5 min of soaking, the impregnated colloidal crystals were transferred to a Büchner funnel, and suction was briefly applied to remove excess solution. These colloidal crystals were introduced into a sealed container, where the precursor was allowed to gel for 1 day at room temperature and aged for another day at 70°C. The 3DOM sol-gel BG was obtained by heating the templated gel at 600°C in air for 1 h (heating rate: 2°C/min). The 600°C thermal treatment is sufficient for organic removal from the sol-gel and thermal decomposition of the PMMA template.³⁰ The calcined product, consisting of millimeter-scale particles, was ground in a mortar and sieved to achieve two different particle size ranges: (1) small particles between 212 and 355 μm and (2) large particles between 600 and 1000 μm. CaO–SiO₂ 3DOM sol-gel BGs with different macropore sizes were prepared by templating the precursor sol with colloid crystals from close-packed monodisperse PMMA spheres of different sizes (average size: 400, 500, and 910 nm).

A CaO–P₂O₅–SiO₂ 3DOM sol-gel bioactive glass was prepared by the same procedure except with the addition of TEP in the precursor solution. A composition of 20 mol % CaO–4% P₂O₅–76% SiO₂ was chosen to study the effect of chemical composition. Table I lists the material parameters of 3DOM sol-gel bioactive glasses prepared for this study.

Soaking in simulated body fluid

In vitro apatite mineralization and glass degradation were evaluated by soaking glass particles in acellular SBF (containing 142.0 mM Na⁺, 5.0 mM K⁺, 2.5 mM Ca²⁺, 1.5 mM Mg²⁺, 148.8 mM Cl⁻, 4.2 mM HCO₃⁻, 1.0 mM HPO₄²⁻ and buffered at pH 7.25 by 50 mM Tris-buffer and 45 mM HCl)¹⁹ at a soaking ratio of 0.1 mg glass/mL simulated body fluid (SBF)³⁰ in polypropylene bottles maintained at 37°C. After selected soaking times, the SBF was sampled, and the solids were separated by vacuum filtration, washed three times with ethanol, and dried in air. The concentrations of Si, P, and Ca in the SBF before and after soaking were analyzed by

inductively coupled plasma (ICP) atomic emission spectroscopy (AES).

Characterization

Samples of 3DOM sol-gel BGs were characterized by nitrogen gas adsorption before soaking in SBF, and by FTIR, XRD, SEM, and TEM before and after soaking in SBF. Nitrogen adsorption measurements were performed on an RXM-100 Catalyst Characterization Instrument (Advanced Scientific Design, Inc.) and specific surface areas were calculated by the Brunauer-Emmett-Teller (BET) method. FTIR spectra were acquired on a Nicolet Magna FTIR 760 spectrometer. The pellets for FTIR were prepared by mixing the dried samples with KBr powder at a weight ratio of 1:32. The XRD study was carried out on a Bruker-AXS microdiffractometer with a 2.2 kW sealed Cu X-ray source. Hitachi S-900 scanning electron microscopes were used to examine the morphology of the samples. Samples for TEM were prepared by ultrasonically dispersing ~5 mg of the powder in 2 mL of absolute ethanol for 10 min and then depositing a few drops of the suspension onto a standard TEM copper grid with a holey carbon support film. TEM images were obtained with a Philips CM30 TEM operating at 300 kV with a LaB₆ filament and recorded with a slow scan CCD camera. The diffraction patterns were obtained at calibrated camera lengths using a NiO_x test specimen as a reference.

RESULTS AND DISCUSSION

Structure before and after soaking in SBF

All sol-gel 3DOM BGs had similar initial microstructural features. This section provides results for the sol-gel 3DOM BG with a composition of 20 mol % CaO–4% P₂O₅–76% SiO₂, small particle size, and 345-nm macropore dimension (345-s-P, see Table I). Subsequent sections reveal the effects of composition, particle size and macropore size on the structural changes on soaking in SBF.

Figure 1 shows SEM images of the phosphate containing 3DOM BG (345-s-P) after calcination. Uniform spherical voids and their surrounding walls form an ordered macroporous structure, in which the array of air spheres exhibits an fcc arrangement.³⁰ The average macropore diameter is 345 nm, somewhat smaller than 400 nm PMMA spherical latex templates. Because the structure has a long-range periodicity with repeat distances overlapping with the wavelength of visible light, the products strongly interacted with light and appeared opalescent. The macropores are interconnected in three dimensions through windows (typical diameters: several tens of nanometers). The highly open, porous structure of 3DOM samples permits free infiltration of liquids, such as SBF. As a result, mate-

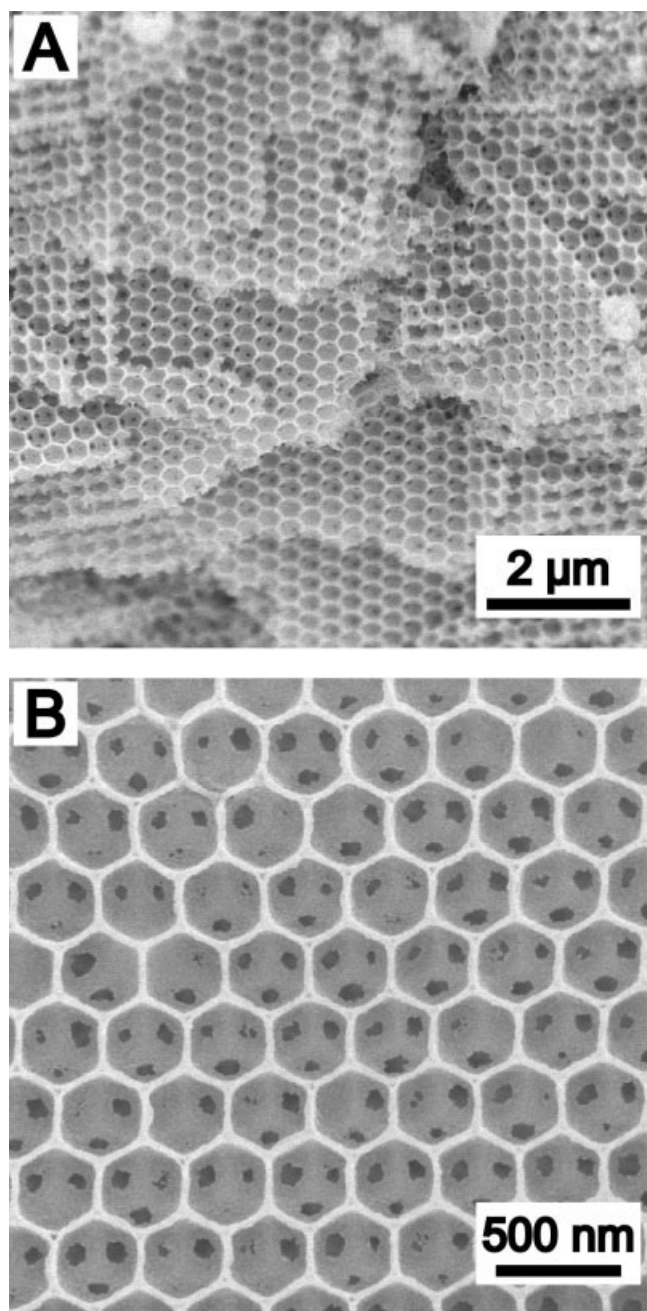


Figure 1. SEM images of a typical 3DOM sol-gel BG (345-s-P) at two different magnifications. The inorganic walls appear as the white and grey areas and windows between pores as dark spots.

materials with 3DOM structure have much larger specific accessible surface areas for liquid media than nonporous solids. The crystallinity of the 3DOM samples was investigated by XRD. No diffraction peaks were observed, indicating an amorphous wall structure.

After soaking this sample in SBF 4 days, the opalescent appearance disappeared, suggesting the loss of the ordered, periodic structure. SEM confirmed this conclusion (see Fig. 2). After soaking in SBF, the glass structure with ordered porosity is gone and a flake-like material is present.

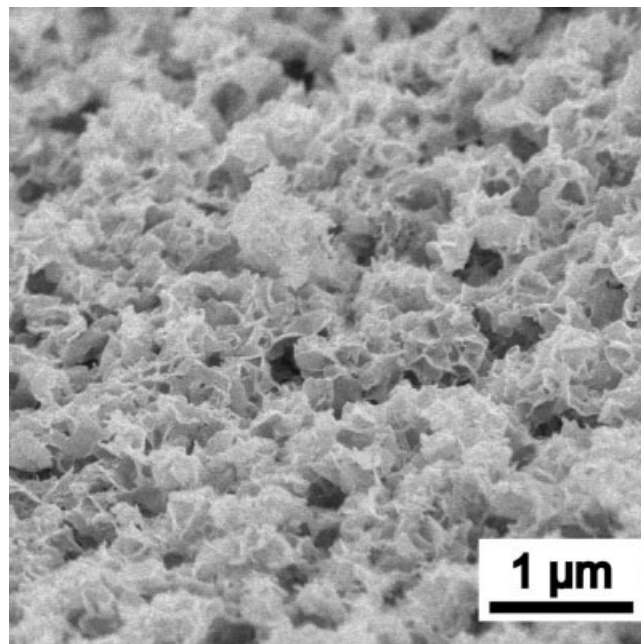


Figure 2. SEM image of a 3DOM sol-gel BG (345-s-P) after soaking in SBF for 4 days.

XRD revealed the crystalline nature of the new material. The diffraction peaks in Figure 3 at approximate d spacings of 3.42 Å (002), 3.08 Å [210], 2.79 Å (broad: (211), (112) and probably (300)) and 2.25 Å (310) are identified as characteristic peaks of bone-like apatite.⁴³ The broadening of the corresponding peaks is due to small grain sizes (see below) and low crystallinity of the mineralized apatite.^{37,43} The apatite structure was also investigated by FTIR. A spectrum is shown in Figure 4. Bands for the phosphate groups (569 cm^{-1} : P—O antisymmetric bending ν_4 ; 604 cm^{-1} : P—O bending ν_4 ; 964 cm^{-1} : P—O stretching ν_1 ; 1041 cm^{-1} : P—O stretching ν_3) and carbonate groups (880 cm^{-1} : C—O stretching ν_4 ; 1422 cm^{-1} : C—O asymmetric

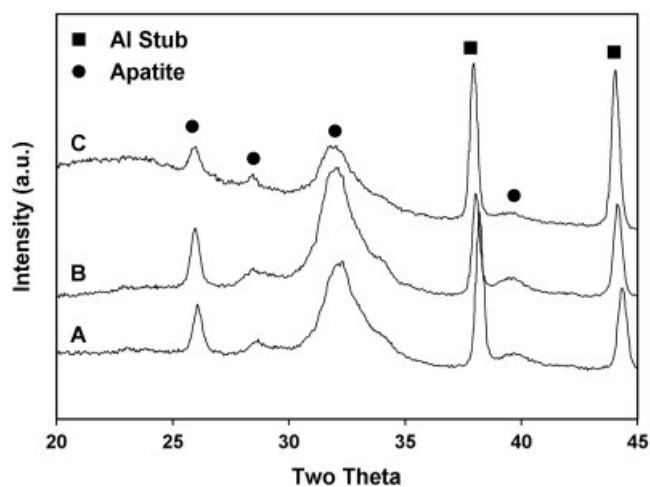


Figure 3. Powder XRD patterns of 3DOM sol-gel BGs after soaking in SBF for 4 days: (A) 345-s-P; (B) 345-s; (C) 345-l.

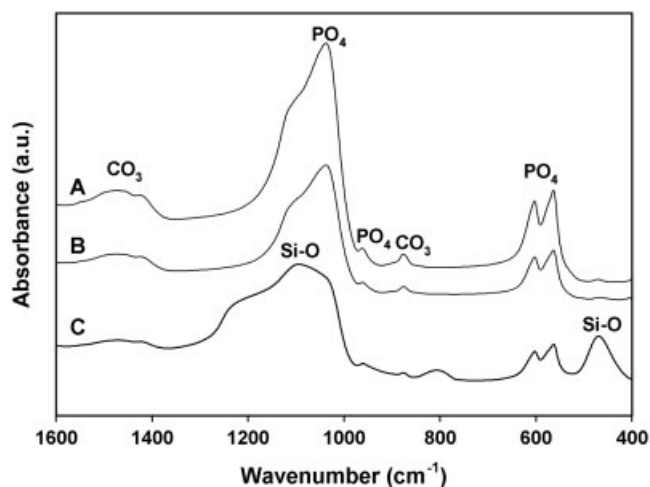


Figure 4. FT-IR spectra of 3DOM sol-gel BGs after soaking in SBF for 4 days: (A) 345-s-P; (B) 345-s; (C) 345-l.

stretching ν_3 ; 1482 cm^{-1} : C—O stretching ν_3)⁴³ are consistent with the spectra for apatite compositions.

The sample after soaking was further analyzed by TEM. The high-magnification image (Fig. 5) shows that the apatite, which appears flake-like in the SEM, is composed of aggregates of nanocrystals with needle shapes 50–100 nm in length. The electron diffraction pattern of the nanocrystals (Fig. 5, inset) shows diffraction rings. The spacings of the rings agree with the characteristic XRD spacings of hydroxyapatite (JCPDS 09-0432). The rings can be assigned to the (002), (211), (310), (222), (213), and (004) planes. In addition, a high-resolution TEM image [Fig. 5(B)] shows the lattice fringes of apatite nanocrystals. The average distance between fringes is 0.82 nm, which is consistent with the value of the {100} interplanar spacing in the apatite structure (0.817 nm). The {100} planes are parallel to the long crystal edge, indicating that the preferential growth direction of apatite is [001].

After soaking in SBF, degradation of the 3DOM glass was apparent in SEM and TEM investigations and was further studied by FTIR of the mineralized products and ICP analysis of the SBF after the soaking period. The FTIR data in Figure 4 shows that in addition to the absorbances for bone-like apatite, a band due to silicate groups in the glass persists (1095 cm^{-1} : Si—O—Si asymmetric stretching ν_3). As will be described below, this absorbance and others for silicate species are stronger for samples that have degraded to a lesser extent. ICP analysis was used to quantify glass degradation (see Table II). The Si concentration of the SBF is increased by 30.2 ppm after 4 days. Considering the total amounts of glass and SBF present initially, the Si concentration would be expected to increase by 34.1 ppm if all of the Si were released from the glass. Therefore, the data shows that ~89% of the Si is released from the 3DOM glass.

Effects of composition

To study glass composition effects, the 3DOM sol-gel BG described in the previous section (20 mol % CaO–4% P₂O₅–76 % SiO₂, 345-s-P) is compared with a 3DOM sol-gel BG having a composition of 20 mol % CaO–80% SiO₂ and identical particle size range and macropore size (345-s).

After soaking the sample (345-s) in SBF for 4 days, both XRD (Fig. 3) and FTIR data (Fig. 4) confirm the

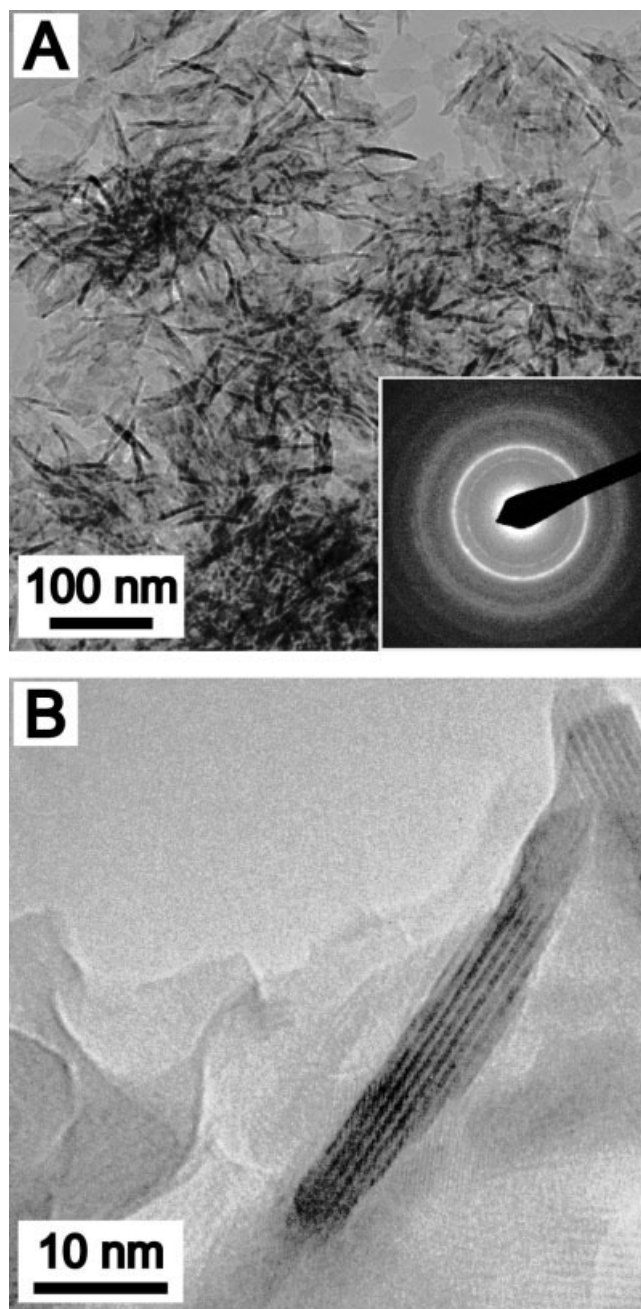


Figure 5. TEM images of a 3DOM sol-gel BG (345-s-P) after soaking in SBF for 4 days: (A) image of flake-like apatite with the corresponding electron diffraction pattern (inset); (B) high-resolution image of an apatite nanocrystal.

TABLE II
Changes in Si, P, and Ca Concentrations of SBF Solutions Exposed to Different 3DOM Sol-gel BGs[†]

Sample	ΔSi (ppm)	ΔP (ppm)	ΔCa (ppm)
345-s-P ^a	30.2	-9.0	-13.6
345-s ^a	30.5	-9.9	-9.9
345-l ^a	22.2	-6.4	-3.0
440-s ^b	29.2	-4.2	2.3
790-s ^b	27.2	-3.7	2.9

[†]Experimental variations in multiple runs were less than 1%.

^aSamples were soaked in SBF for four days.

^bSamples were soaked in SBF for two days.

formation of bone-like apatite for the CaO-SiO₂ 3DOM sol-gel BG, consistent with previous results.³⁰ SEM results (not shown) reveal the formation of the flakey bone-like apatite and the disappearance of the ordered macroporous glass structure, similar to that shown in Figure 2. Quantitative comparison of apatite formation is challenging. Vallet-Regi et al.²⁶ reported that larger apatite crystals formed on a sol-gel glass with a composition of 17 mol % CaO-3% P₂O₅-80% SiO₂ after soaking in SBF for 7 days compared with a phosphorus-free glass (20 mol % CaO-80% SiO₂). Microstructural differences in the apatite formed on the glasses in this study were not easily discerned. Other variables such as particle size and macropore size appear to have more important effects, as described below.

Differences in degradation were not apparent in the FTIR data or SEM images; however, ICP data (see Table II) showed that after 4 days in SBF, ~81% of Si was released for 345-s compared with ~89% for 345-s-P sample. Thus, the CaO-P₂O₅-SiO₂ glass appears to have degraded slightly more than CaO-SiO₂ glass.

Effects of glass particle size

Two different particle sizes of the 20 mol % CaO-80% SiO₂ (345-s and 345-l) were prepared to explore particle size effects on apatite formation and glass degradation. Figure 6 shows SEM images of these samples after soaking in SBF for 4 days. The morphology of the two samples is quite different. For small glass particles (345-s), flake-like apatite could be found throughout the sample [Fig. 6(A)]. In contrast, for large glass particles (345-l), remnants of the templated 3DOM glass were still visible [Fig. 6(B)], suggesting less glass degradation. XRD patterns (Fig. 3) confirm that bone-like apatite was present in both samples.

To qualitatively understand glass degradation and mineralization, FTIR and ICP studies were conducted. The FTIR data in Figure 4 shows that in addition to the absorbances for bone-like apatite (bands of phosphate

groups: 569, 604, 964, 1041 cm⁻¹; carbonate groups: 880, 1422, 1482 cm⁻¹), strong bands due to silicate groups (474 cm⁻¹: Si-O-Si bending ν_4 ; 802 cm⁻¹: Si-O symmetric stretching ν_3 ; 1095 cm⁻¹: Si-O-Si asymmetric stretching ν_3) are present for large particles (345-l, Fig. 4). The silicate peaks are much less pronounced in the sample with smaller particle size (345-s, Fig. 4), indicating more complete degradation. ICP analysis further revealed the difference in glass degradation (see Table II). For large particles (345-l), the Si concentration of the SBF was increased by 22.2

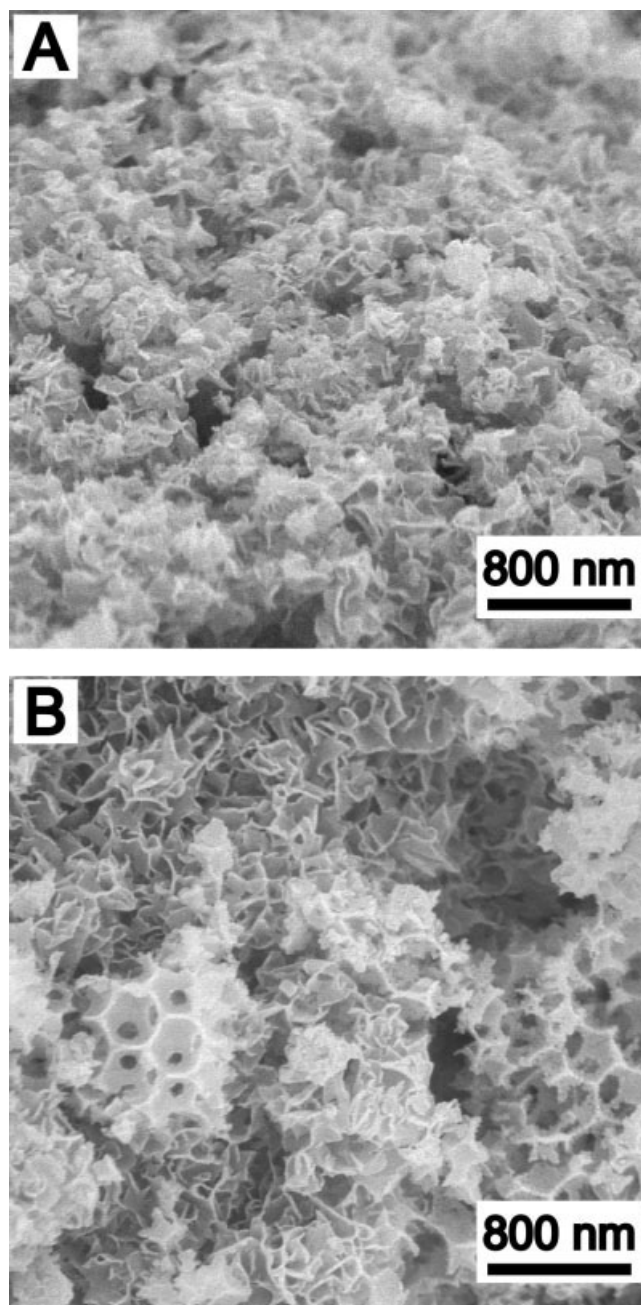


Figure 6. SEM images of 3DOM sol-gel BGs with composition 20 mol % CaO-80% SiO₂ after soaking in SBF for 4 days: (A) small particles (345-s); (B) large particles (345-l).

ppm after 4 days, corresponding to 59% of the Si released from the 3DOM glass. In comparison, 81% of Si was released from the small glass particles (345-s). Additionally, phosphorous depletion from SBF was less for large particle sample (345-l) compared with that for the small particle sample (345-s). Because the phosphorous in SBF is consumed during the development of apatite, one can calculate that ~50% more apatite formed in the case small particles.

The above results demonstrate that the amount of glass degradation and apatite formation was greater for the 3DOM glass with smaller particle size. Similar results were reported by Sepulveda et al.¹² for a conventional melt-derived BG and a sol-gel BG particles; however, due to differences between materials used in Sepulveda's study and those in the present study, the observed particle size effects are likely caused by different processes. For conventional melt-derived and sol-gel BGs, mass transport and ion exchange, which are directly related to glass degradation and mineralization, mainly occur at the geometric surfaces of the particles. The smaller the particle size, the larger is the contact surface area with SBF and the number of nucleation sites, leading to faster degradation and mineralization. Mesoporosity in the sol-gel BG has the effect of speeding the dissolution and formation of the apatite layer compared with the dense melt-derived BG.¹² For 3DOM sol-gel BGs, the macropores play another role, allowing mass transport and ion exchange to occur not only at external surfaces (outside geometric surface of the particle) but also at internal surfaces (macropore surface within the particles). For these porous materials, the external surface area is only a small fraction of the total accessible surface area (external and internal surface areas).

The importance of interior surfaces is revealed in Figure 7. After 2 days' soaking in SBF a bone-like apatite has grown from the pore walls into the pore space to form a regular spherical apatite array. This interesting structure was found in all samples after 2 days' soaking. It appeared at different locations in the particulate samples, but not uniformly throughout, indicating that decomposition and mineralization depend on the local conditions inside and around the particle. Such nonuniformity contributes to the observed particle size effect.

When the 3DOM sol-gel BGs are placed in SBF, the SBF freely infiltrates the macroporous network. Then, reactions for dissolution and calcium phosphate deposition are initiated on all surfaces, and the composition of the fluid filling the macroporous network changes. Ionic diffusion in the fluid ensues with dissolved silicate species leaving and calcium and phosphorous ions entering the macroporous network. The time needed for this diffusion is longest for the surfaces in the innermost portions of the particle. Hence, one expects that the interior surfaces, deepest in the

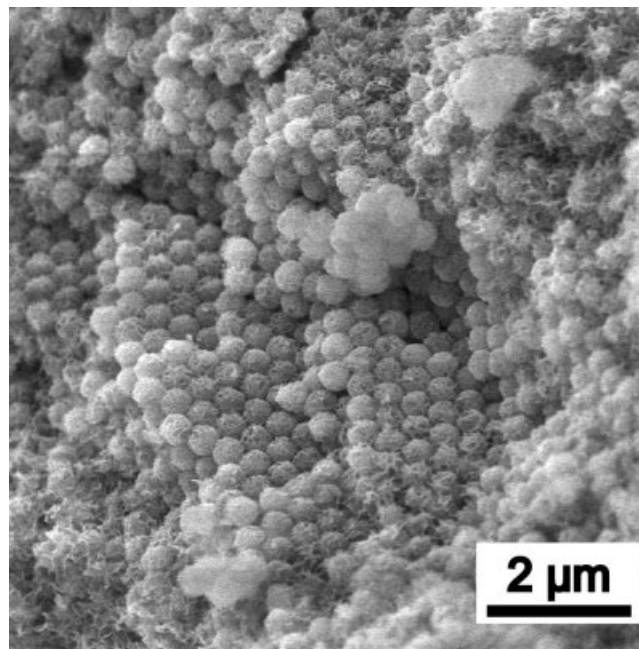


Figure 7. SEM images of 3DOM sol-gel BGs (440-s) with composition 20 mol % CaO–80% SiO₂ after soaking 2 days in SBF.

particle, will degrade and form apatite more slowly compared with those nearer to the bulk SBF fluid phase. In addition, the formation of apatite on the external and internal surfaces over time has the effect of cutting off the fluid in the interior of macroporous network from the bulk of the SBF. Thus, after a given amount of time in SBF, larger 3DOM particles degrade less completely and form less apatite.

Effects of macropore size

In addition to particle size, the macropore size is an important structural parameter. Two 3DOM sol-gel BG samples with a composition of 20 mol % CaO–80% SiO₂ were prepared using PMMA templates with different sphere sizes. Based on SEM measurements, the macropore sizes for these samples were 440 and 790 nm, respectively (Fig. 8). Although more difficult to quantify, the wall thicknesses especially at the interstices between the PMMA particles are thicker when larger latex spheres are used. Before further evaluation, both samples were sieved to achieve the small particle size range and were labeled 440-s and 790-s, respectively.

After soaking these samples in SBF for 2 days, the formation of apatite flakes was observed by SEM and the bone-like apatite phase confirmed by XRD for both samples (data not shown). The shorter soaking time was used in this case in order to better capture the earlier development of structure. According to the

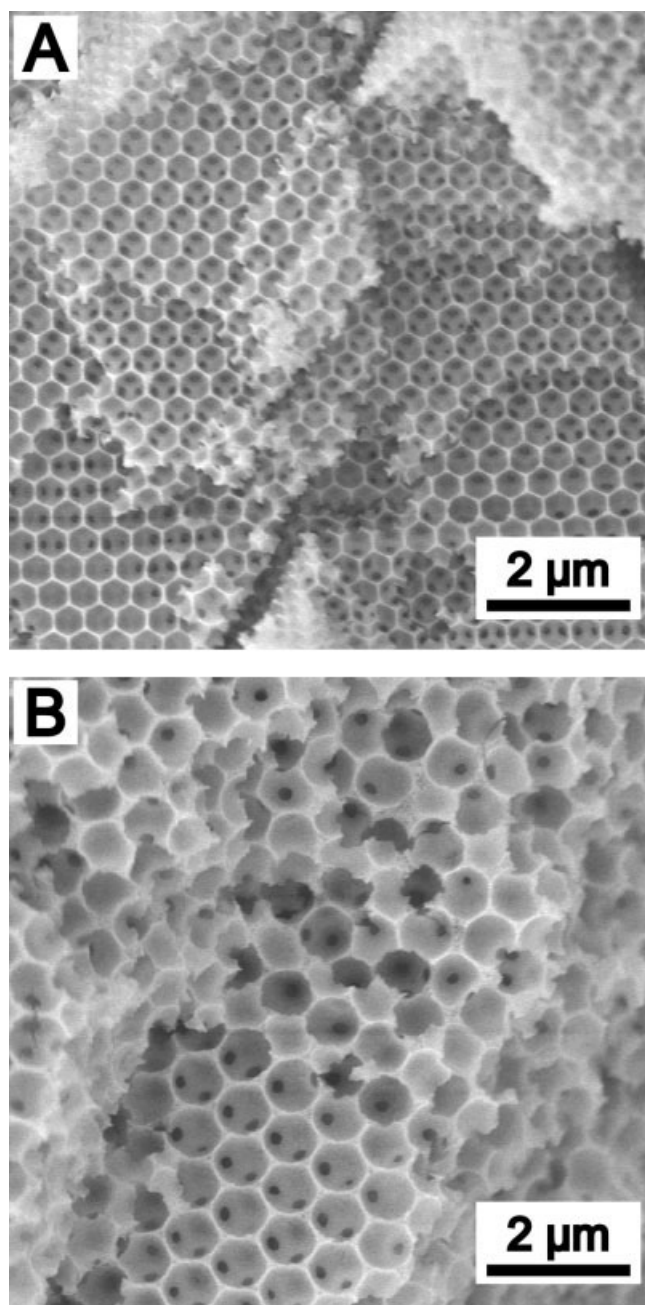


Figure 8. SEM images of 3DOM sol-gel BGs with composition 20 mol % CaO–80% SiO₂ and two different average macropore sizes: (A) 440 nm (440-s); (B) 790 nm (790-s).

SEM images, more 3DOM sol-gel BG remains in the large-pore sample (790-s). Figure 9 shows the FTIR spectra of both samples after soaking. The appearance of typical bands for phosphate groups and carbonate groups provide further evidence for the formation of apatite in both samples. However, the spectrum of the large-pore sample (790-s) showed a larger Si—O—Si absorption at 474 cm⁻¹, indicating a greater amount of silicate remaining in the structure. This result was confirmed by ICP analysis. About 72% of Si was released from the large-pore sample (790-s) after 2 days

compared with 77% of Si for the small-pore sample (440-s). In addition, the phosphorous depletion is greater for the smaller-pore sample, indicating more apatite formation in this case.

The formation of apatite on sol-gel BGs is strongly affected by the pore structure. Previous studies have focused on the effects of mesopores. Pereira et al.²¹ suggested that a mesopore size of at least 2 nm was required to form apatite on sol-gel BGs. Another study³⁴ indicated that a large mesopore volume and a wide mesopore size distribution favor hydroxycarbonate apatite nucleation. The effects of the macropores have not been studied as completely; our previous report demonstrated that a macroporous structure can be beneficial for apatite formation in SBF.³⁰ The current investigation shows that the extents of apatite mineralization and glass degradation after 2 days in SBF increase with decreasing macropore size. This observation can be explained by the variation of the surface area accessible to SBF. Generally, the larger the accessible surface area, the larger is the number of nucleation sites and hence the mineralization rate. For 3DOM structures, the specific accessible surface area in a given volume of material is inversely proportional to the macropore size. Based on nitrogen adsorption data, the BET surface areas of the 440- and 790-s samples were 105 and 81 m²/g, respectively. Although a large portion of the BET surface area is due to mesoporosity in sol-gel BGs, we believe that the difference in surface area between these two samples is partially caused by a variation in macropore size. Hence the 3DOM sol-gel BG with smaller macropores exhibits more glass degradation and apatite mineralization after 2 days in SBF. More research is needed to determine if this pore size effect is significant after longer soaking times and to determine the effect of macropore size over a wider pore size range.

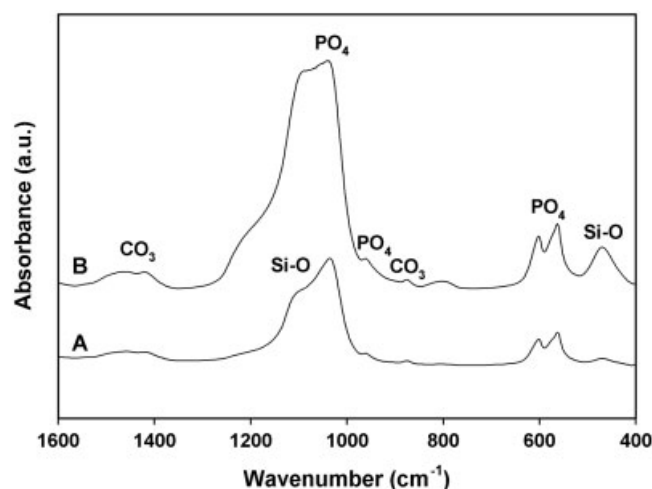


Figure 9. FT-IR spectra of 3DOM sol-gel BGs with composition 20 mol % CaO–80% SiO₂ after soaking in SBF for 2 days: (A) 440-s; (B) 790-s.

Although materials parameters affect *in vitro* mineralization and degradation of 3DOM sol-gel BGs in SBF, it is still unknown if similar effects will hold *in vivo*. Future work will require the assessment of 3DOM sol-gel BGs *in vitro* and *in vivo* performance in cell culture and animal models, respectively.

SUMMARY

3DOM sol-gel BGs with different compositions, particle sizes, and macropore sizes were prepared by colloidal crystal templating. *In vitro* glass degradation and apatite mineralization in acellular simulated body fluid (SBF) were studied. The experiments demonstrated that degradation of 3DOM sol-gel BGs and mineralization to apatite are processes that benefit from the accessible surfaces in 3DOM structures and from facile diffusion of SBF through these porous solids. The studies also showed that these processes are influenced by material parameters. Within the parameter range of these experiments, smaller particle sizes and macropore sizes result in more glass degradation and apatite mineralization. Incorporation of 4 mol % P₂O₅ in 3DOM SiO₂-CaO BGs had a minor effect of increasing the amount of degradation. Because the interactions between these parameters are complex, the parameters need to be optimized together to achieve the best performance of a 3DOM sol-gel BG.

References

- Hench LL. Bioceramics. *J Am Ceram Soc* 1998;81:1705-1728.
- Hench LL, West JK. Biological applications of bioactive glasses. *Life Chemistry Report* 1996;13:187-241.
- Hench LL. Bioactive materials: the potential for tissue regeneration. *J Biomed Mater Res* 1998;41:511-518.
- Zhang K, Ma Y, Francis LF. Porous polymer/bioactive glass composites for soft-to-hard tissue interfaces. *J Biomed Mater Res* 2002;61:551-563.
- Kokubo T. Bioactive glass ceramics: properties and applications. *Biomaterials* 1991;12:155-163.
- Sepulveda P, Jones JR, Hench LL. Bioactive sol-gel foams for tissue repair. *J Biomed Mater Res* 2002;59:340-348.
- Hench LL, Polak JM. Third-generation biomedical materials. *Science* 2002;295:1014-1017.
- Brinker CJ, Scherer GW. *Sol-gel science: the physics and chemistry of sol-gel processing*. New York: Academic Press; 1990.
- Li R, Clark AE, Hench LL. Effects of structure and surface area on bioactive powders by sol-gel process. In: Hench LL, West JK, editors. *Chemical processing of advanced materials*. New York: John Wiley and Sons; 1992. p 627-633.
- Li P, Ohtsuki C, Kokubo T, Nakanishi K, Soga N. Apatite formation induced by silica gel in a simulated body fluid. *J Am Ceram Soc* 1992;75:2094-2097.
- Pereira MM, Clark AE, Hench LL. Calcium phosphate formation on sol-gel-derived bioactive glasses *in vitro*. *J Biomed Mater Res* 1994;28:693-698.
- Sepulveda P, Jones JR, Hench LL. *In vitro* dissolution of melt-derived 45S5 and sol-gel derived 58S bioactive glasses. *J Biomed Mater Res* 2002;61:301-311.
- Wheeler DL, Eschbach EJ, Hoellrich RG, Montfort MJ, Chamberland DL. Assessment of resorbable bioactive material for grafting of critical-size cancellous defects. *J Orthopaedic Res* 2000;18:140-148.
- Hamadouche M, Meunier A, Greenspan DC, Blanchat C, Zhong JP, La Torre GP, Sedel L. Bioactivity of sol-gel bioactive glass coated alumina implants. *J Biomed Mater Res* 2000;52:422-429.
- Hamadouche M, Meunier A, Greenspan DC, Blanchat C, Zhong JP, La Torre GP, Sedel L. Long-term *in vivo* bioactivity and degradability of bulk sol-gel bioactive glasses. *J Biomed Mater Res* 2001;54:560-566.
- Santos EM, Radin S, Ducheyne P. Sol-gel derived carrier for the controlled release of proteins. *Biomaterials* 1999;20:1695-1700.
- Radin S, Ducheyne P, Kamplain T, Tan BH. Silica sol-gel for the controlled release of antibiotics I. synthesis, characterization, and *in vitro* release. *J Biomed Mater Res* 2001;57:313-320.
- Livage J, Coradin T, Roux C. Encapsulation of biomolecules in silica gels. *J Phys Condens Matter* 2001;13:R673-R691.
- Kokubo T, Kushitani H, Sakka S, Kitugi T, Yamanuro T. Solutions able to reproduce *in vivo* surface-structure changes in bioactive glass-ceramic A-W. *J Biomed Mater Res* 1990;24:721-734.
- Li P, Ohtsuki C, Kokubo T, Nakanishi K, Soga N, de Groot K. The role of hydrated silica, titania, and alumina in inducing apatite on implants. *J Biomed Mater Res* 1994;28:7-15.
- Pereira MM, Clark AE and Hench LL. Effect of texture on the rate of hydroxyapatite formation on gel-silica surface. *J Am Ceram Soc* 1995;78:2463-2468.
- Pereira MM and Hench LL. Mechanisms of hydroxyapatite formation on porous gel-silica substrates. *J Sol-Gel Sci Tech* 1996;7:59-68.
- Li P, Nakanishi K, Kokubo T and De Groot K. Induction and morphology of hydroxyapatite, precipitated from metastable simulated body fluids on sol-gel prepared silica. *Biomaterials* 1993;14:963-968.
- Ramila A, Vallet-Regi M. Static and dynamic *in vitro* study of a sol-gel glass bioactivity. *Biomaterials* 2001;22:2301-2306.
- Ramila A, Balas F, Vallet-Regi M. Synthesis routes for bioactive sol-gel glasses: alkoxides versus nitrates. *Chem Mater* 2002;14:542-548.
- Vallet-Regi M, Izquierdo-Barba I, Salinas AJ. Influence of P₂O₅ on crystallinity of apatite formed *in vitro* on surface of bioactive glasses. *J Biomed Mater Res* 1999;46:560-565.
- Vallet-Regi M, Salinas AJ, Roman J, Gil M. Effect of magnesium content on the *in vitro* bioactivity of CaO-MgO-SiO₂-P₂O₅ sol-gel glasses. *J Mater Chem* 1999;9:515-518.
- Laczka M, Cholewa-Kowalaska K, Laczka-Osyczka A, Tworzyno M, Turyna B. Gel-derived materials of a CaO-P₂O₅-SiO₂ system modified by boron, sodium, magnesium, aluminum, and fluorine compounds. *J Biomed Mater Res* 2000;52:601-612.
- Jokinen M, Rahiala H, Rosenholm JB, Peltola T, Kangasniemi I. Relation between aggregation and heterogeneity of obtained structure in sol-gel derived CaO-P₂O₅-SiO₂. *J Sol-Gel Sci Tech* 1998;12:159-167.
- Yan H, Zhang K, Blanford CF, Francis LF, Stein A. *In vitro* hydroxycarbonate apatite mineralization of CaO-SiO₂ sol-gel glasses with a three-dimensionally ordered macroporous structure. *Chem Mater* 2001;13:1374-1382.
- Arcos D, Greenspan DC, Vallet-Regi M. Influence of the stabilization temperature on textural and structural features and ion release in SiO₂-CaO-P₂O₅ sol-gel glasses. *Chem Mater* 2002;14:1515-1522.
- Cho SB, Nakanishi K, Kokubo T, Soga N, Ohtsuki C, Nakamura T, Kitsugi T, Yamamuro T. Dependence of apatite for-

- mation on silica gel on its structure: effect of heat treatment. *J Am Ceram Soc* 1995;78:1769–1774.
33. Martinez A, Izquierdo-Barba I, Vallet-Regi M. Bioactivity of a CaO-SiO₂ binary glasses system. *Chem Mater* 2000;12:3080–3088.
 34. Peltola T, Jokinen M, Rahiala H, Levanen E, Rosenholm JB, Kangasniemi I, Yli-Urpo A. Calcium phosphate formation on porous sol-gel-derived SiO₂ and CaO-P₂O₅-SiO₂ substrates in vitro. *J Biomed Mater Res* 1999;44:12–21.
 35. Perez-Pariente J, Balas F, Roman J, Salinas AJ, Vallet-Regi M. Influence of composition and surface characteristic on the in vitro bioactivity of SiO₂-CaO-P₂O₅-MgO sol-gel glasses. *J Biomed Mater Res* 1999;47:170–175.
 36. Perez-Pariente J, Balas F, Vallet-Regi M. Surface and chemical study of SiO₂-P₂O₅-CaO (MgO) bioactive glasses. *Chem Mater* 2000;12:750–755.
 37. Vallet-Regi M, Arcos D, Perez-Pariente J. Evolution of porosity during in vitro hydroxycarbonate apatite growth in sol-gel glasses. *J Biomed Mater Res* 2000;51:23–28.
 38. Vallet-Regi M, Ramila A. New bioactive glass and changes in porosity during the growth of a carbonate hydroxyapatite layer on glass surfaces. *Chem Mater* 2000;12:961–965.
 39. Viitala R, Jokinen M, Peltola T, Gunnelius K, Rosenholm JB. Surface properties of in vitro bioactive and non-bioactive sol-gel derived materials. *Biomaterials* 2002;23:
 40. Stein A, Schroden RC. Colloidal crystal templating of three-dimensionally ordered macroporous solids-materials for photonics and beyond. *Curr Opin Solid State Mater Sci* 2001;5:553–564.
 41. Yan H, Blanford CF, Holland BT, Smyrl WH, Stein A. General synthesis of periodic macroporous solids by templated salt precipitation and chemical conversion. *Chem Mater* 2000;12:1134–1141.
 42. Yan H, Blanford CF, Holland BT, Parent M, Smyrl WH, Stein A. A chemical synthesis of periodic macroporous NiO and metallic Ni. *Adv Mater* 1999;11:1003–1006.
 43. LeGeros RZ. Calcium phosphates in oral biology and medicine. *Monogr Oral Sci* 1991;15:1–192.